J. Adhesion Sci. Technol., Vol. 17, No. 14, pp. 1923–1944 (2003)

Also available online - www.vsppub.com

Adhesion characteristics of underfill resins with flip chip package components

MAN-LUNG SHAM and JANG-KYO KIM *

Department of Mechanical Engineering, Hong Kong University of Science and Technology, Clear Water Bay, Kowloon, Hong Kong

Received in final form 19 August 2003

Abstract—Of fundamental importance to enhance the reliability of flip chip on board (FCOB) packages is to avoid the initiation and propagation of various interfacial failures and, therefore, robust interfacial bonds between the underfill and other components are highly desired. In the present study, the interfacial bond strengths of both conventional and no-flow underfill resins with die passivation, eutectic solder and epoxy solder mask are measured using the button shear test. The surface characteristics of these substrates are analyzed using various techniques, including optical scanning interferometry, scanning electron microscopy and contact angle measurements. It is found that the interfacial bond strength of the underfill with the eutectic solder is far weaker than of other interfaces. The degradation of underfill bond strength with silicon nitride passivation, eutectic solder and polymeric solder mask surfaces is enhanced in the presence of solder flux, and cleaning the fluxed surface with a saponifier is an efficient means to restore the original interfacial adhesion. The necessity of post-solder reflow cleaning is shown by performing thermal cycle tests on FCOB packages with different extents of flux residue. Distinctive solder failure behaviors are observed for the packages with and without post-solder reflow cleaning from the cross-sectional analysis.

Keywords: Flip chip; interfacial adhesion; underfill resin; solder; solder mask; passivation layer.

1. INTRODUCTION

Flip-chip technology has attracted significant attention in the electronic packaging industry. A flip chip on board (FCOB) package consists of a silicon die and a printed circuit board (PCB), which are interconnected using solder balls, and an underfill resin is dispensed along the die edges to fill up the small gap between

*To whom correspondence should be addressed. Phone: (852) 2358-7207. Fax: (852) 2358-1543. E-mail: mejkkim@ust.hk

the die and the PCB. A schematic diagram of a typical FCOB package is shown in Fig. 1. The underfill resin reduces the relative displacement between the die and the PCB and, thus, the stresses in the solder interconnection that arise from thermal cycling and mechanical loading are reduced. Other functions of the underfill include protection of solder joints and silicon dies from environmental attack and harmful α-particle emission originating from the radioactive impurities present in the lead–tin solder. With the ever-increasing applications of low-cost flip-chip packages, various types of underfill materials have been developed to further improve the production throughput. These include fast-flow underfill, snap-cure underfill, reworkable underfill and no-flow underfill resins.

Although the use of underfill encapsulation significantly enhances the reliability of a solder–joint interconnection, weak interfacial adhesion and delamination between the underfill and other package components are a major concern. Delamination of underfill may force the solder balls to withstand the majority of deformation of the package assembly during cyclic loading, leading to premature shear failure. Delamination also results in accumulation of moisture at the failed interfaces leading to additional failure modes. This suggests that the reliability of flip-chip devices depends not only on the properties of underfill but also on the integrity of the interfaces between the underfill and various package components, such as die passivation [1–3], solder mask [3, 4] and solder joint surface [5]. To reduce the possibility of delamination initiation and propagation, many measures have been taken [6], including appropriate process controls to minimize void formation in the underfill resin, reduction of mismatches in thermo-mechanical properties between the adjacent components, proper design of package geometry, as well as improvement of interfacial bond strength between the components. Typical approaches devised to enhance the interfacial adhesion between the polymeric encapsulants and other package components include incorporating a silane coupling agent in the underfill resin [7–9] and surface modification of the package components via plasma

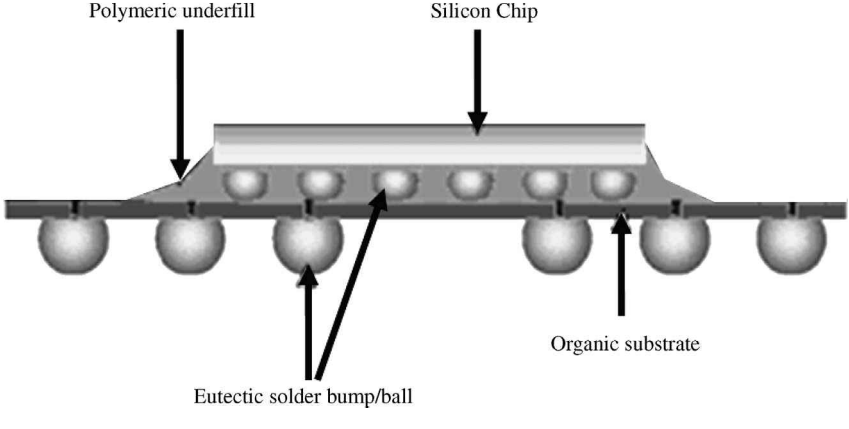

Figure 1. Schematic diagram of flip chip on board (FCOB) package.

[10–12] or UV/ozone treatment [13]. Besides, die edge cracking and underfill fillet cracking are also frequently reported during the thermal cycling tests, in particular the underfill cracking at the die corner due to the significantly high stress concentration [6].

Another important issue arising from the FCOB assembly process is the use of flux. An organic rosin-based flux is usually applied onto the flip-chip components to clean the component surface and reduce oxidation during the high temperature solder reflow process, which are necessary to facilitate proper wetting of metallization pads by the solder. The flux residue remains on the package component surface after the assembly process. While leaving the flux residue without further cleaning is an acceptable practice in the industry, the presence of flux residue can cause serious problems, such as incomplete filling of underfill introducing voids around the solder balls and incomplete wetting of substrate surfaces by the underfill resin, resulting in weak interfacial adhesion.

The objective of this work was to identify the interfacial adhesion characteristics between the underfill and the flip-chip package components, including silicon die passivation, epoxy-based solder mask and eutectic solder. Special emphasis was placed on the evaluation of interfacial adhesion before and after cleaning the fluxed surfaces. To evaluate the importance of removing the flux residue prior to encapsulation by the underfill, the interfacial bond strengths of the underfill with package components with flux residue were measured. The same measurements were made after cleaning using a saponifier to study whether the saponifier was efficient to restore the original surface quality. Accelerated thermal cycling test was also performed on the FCOB package to illustrate the significance of post-solder reflow cleaning.

2. EXPERIMENTAL

2.1. Materials and specimen preparation for button shear test

Two conventional and two no-flow underfill resins (supplied by Henkel Loctite and National Starch, respectively) were processed according to the curing conditions given in Table 1. The conventional underfill resins are known to contain silica fillers approx. 50–70 wt%, whereas the no-flow underfill resins contain reactive liquid rubber modifiers. Concerning the effect of curing profile on the no-flow underfill,

Table 1.
Curing conditions for the underfills used

Underfill	Conventional		No-flow	
	UF A	UF B	UF C	UF D
Curing temperature (°C)	160	150	165	165
Curing time (min)	7	30	20	20

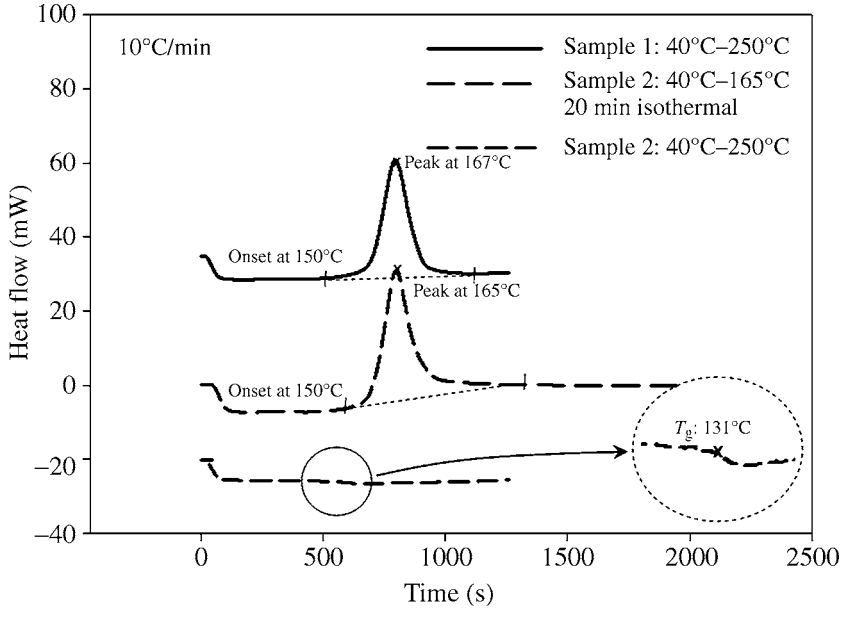

Figure 2. Differential scanning calorimetry (DSC) measurement on the completeness of curing of no-flow underfill (UF C) under 165°C/20 min condition. The curing cycle of Sample 1 was from 40°C to 250°C, 10°C/min, and the curing cycle of Sample 2 was from 40°C to 165°C, 20 min isothermal at 165°C.

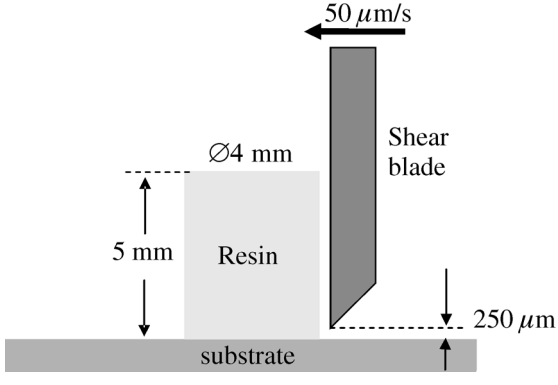

Figure 3. Schematic drawing of the button shear test.

it is found that the onset temperature of the exothermic reaction in the current no-flow underfill (UF C) was about 150°C as shown in Fig. 2. When the curing cycle was carried out at 250°C with a 10°C /min ramp rate, curing at 165°C for 20 min was sufficient to cure the no-flow underfill completely, because no residual heat was noticed upon heating of the same sample to 250°C.

The button shear test [14] was performed to measure the interfacial bond strength between the underfill resin and the package components. The specimens were prepared by molding a cylindrical resin block of 4 mm in diameter and 5 mm in

Table 2.
Substrates investigated for the adhesion test

Substrate	Specifications
Solder mask	Taiyo 4000 (AUS-5) solder mask on FR-4 of 35 μm in thickness
Eutectic solder plate	63/37 Sn/Pb, 1 mm in thickness
SiO_2 passivation	Passivation layer 0.75 μm thick on the bare Si die of 525 μm thickness
Si_3N_4 passivation	Passivation layer 0.75 μm thick on the bare Si die of 525 μm thickness
Benzocyclobutene (BCB) passivation	Passivation layer 5 μm thick on the bare Si die of 525 μm thickness

height, using a Teflon mold. Figure 3 shows the schematic diagram of the button shear test. A shear load was applied at a speed of 50 μm/s using a blade 250 μm above the substrate surface on a Dage 4000 Multi-purpose Bond Tester, and the maximum force corresponding to delamination of the resin button from the substrate was recorded. At least 8 specimens were tested for a given set of conditions. The maximum shear stress was used to calculate the interfacial bond strength that was defined by the maximum force divided by the circular contact surface area.

The package components studied included an eutectic solder, epoxy-based solder mask and three different types of passivation layers. The compositions/specifications of these substrate materials are summarised in Table 2. The solder specimen was prepared by melting the 63% Sn/37% Pb eutectic solder balls and moulding to form 1-mm-thick solder plate. The two-part photo-imageable epoxy-based solder mask (Taiyo America, PSR-4000 (AUS 5)) was cured at 149°C for 1 h. The deposition of silicon dioxide (SiO_2) and silicon nitride (Si_3N_4) over the silicon wafer was carried out using a STS 310 plasma enhanced chemical vapour deposition system (PECVD). The benzocyclobutene (BCB) passivation layer was prepared by spin coating BCB liquid resin on a silicon wafer, followed by curing at 240°C for 40 min.

2.2. Flip-chip fabrication and effect of flux residue

To study the effect of flux residue on the interfacial adhesion, a 20-μm-thick rosin-based flux (Kester TSF-6502) was stencil printed on the solder mask, solder and Si_3N_4 passivation surfaces. The flux-coated solder mask and Si_3N_4 specimens were subjected to a typical 6-min solder reflow cycle involving a peak temperature of 215°C, whereas the flux coated solder substrate assembly was heated at 170°C for 1 h to avoid re-melting of the eutectic solder. The flux weight losses for the two temperature profiles obtained from a thermogravimetric analyzer (TGA) are shown in Fig. 4. It was found that the weight loss of flux under the 170°C/h condition was much higher than in a typical 6-min solder reflow with a peak temperature of 210°C. This suggests that the temperature profile used in this study might underestimate the actual degradation of the interfacial bond between the underfill and solder plate, which can be caused by the flux residue after a typical solder reflow profile.

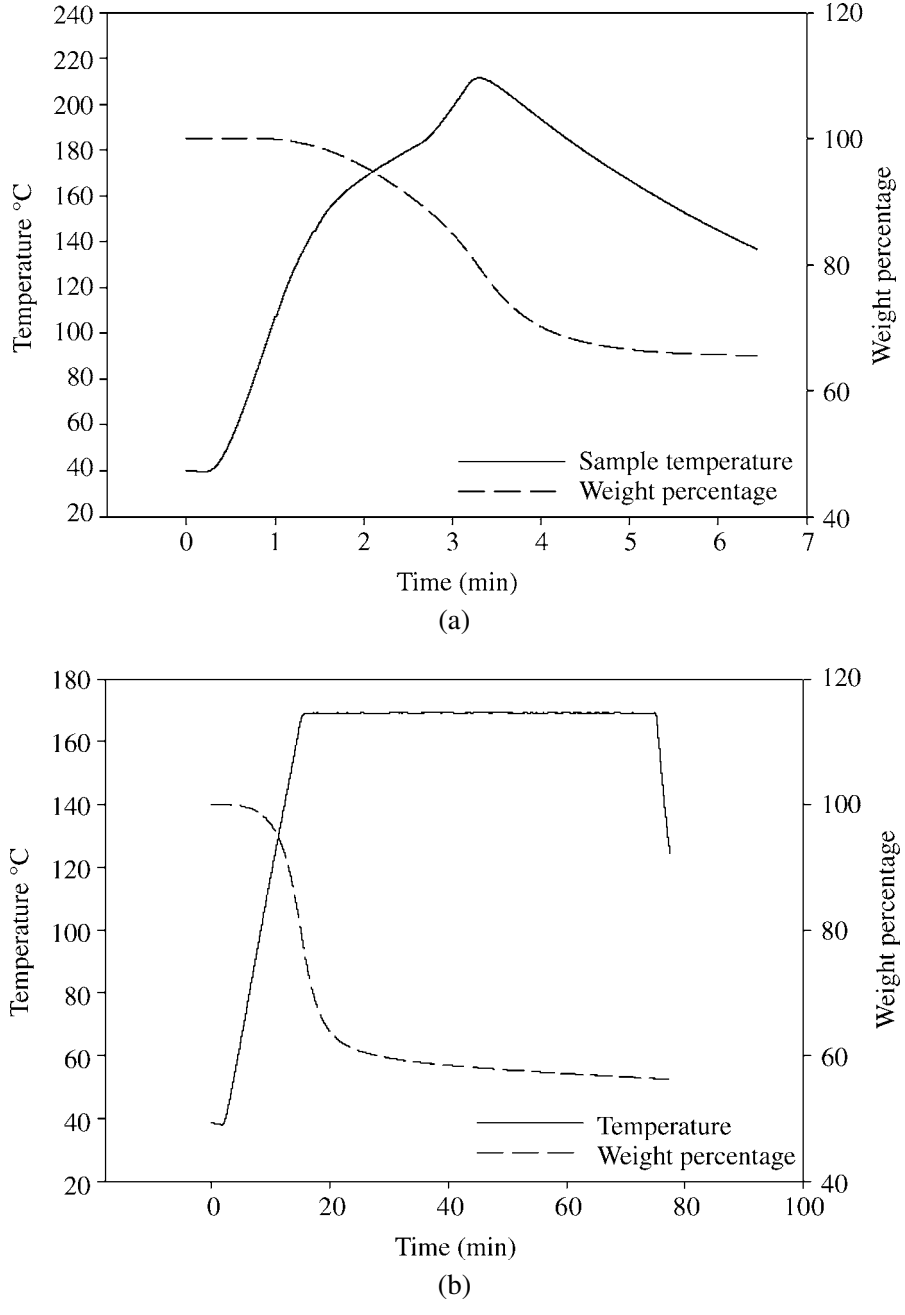

Figure 4. Effect of thermal conditions on the weight of flux residue (Kester TSF-6502): (a) under a reflow cycle and (b) under 170°C for 1 h.

The interfacial adhesion of the underfill to cleaned substrate surfaces was evaluated after removing the flux residue. The flux was removed using an alkaline saponifier containing diglycolamine, which can convert the rosin-based flux into a water-soluble soap by the saponfication process as shown below [15]:

$$\text{Saponification: Base} + \text{RCOOH} \rightarrow \underset{\text{Insoluble rosin flux}}{\text{H}^+/\text{Base}} + \underset{\text{Water-soluble flux}}{\text{RCOO}^-} \tag{1}$$

The cleaned surfaces were then rinsed with DI water and dried before moulding a cylindrical resin block for the button shear test. The FCOBs with and without post-cleaning before underfill encapsulation were also prepared by assembling the 550-μm-thick flip chip on 200-μm-thick bismaleimide triazine (BT) substrate, and the bump height and diameter were 70 μm and 200 μm, respectively. The applied flux and underfill during the assembly were Kester TSF-6502 and UF A, respectively. The FCOBs were subjected to 1000 cycles of accelerated thermal (AT) load between -40 and $+125^\circ$C with the ramp and dwell periods of 15 min each in a chamber. Both non-destructive and destructive examinations were performed. A scanning acoustic microscope (SONIX L/HF 200) was used to monitor the generation and growth of voids in the package after an AT test. The package after being subjected to an AT test was cross-sectioned using a diamond saw and the surface polished, which was then examined under a scanning electron microscope (JEOL 6300).

2.3. Surface characterization

The surface free energies of the substrates were evaluated to correlate with the interfacial bond strength with underfill resins. The contact angles on the substrate surfaces, θ, were measured using two test liquids, namely de-ionized (DI) water and methylene iodide, on a Krüss G10 contact angle measuring system. The contact angles were recorded after about 15 s from the liquid dispensing to ensure that the droplet had reached an equilibrium state. At least 10 measurements were made for each set of conditions, and the average values were used to calculate the surface free energies. The polar and non-polar (or dispersive) components, γ_s^p and γ_s^d, respectively, of the solid surface free energy were determined based on the harmonic-mean approach [16].

$$\gamma_l(1+\cos\theta) = \frac{4\gamma_s^d\gamma_l^d}{\gamma_s^d+\gamma_l^d} + \frac{4\gamma_s^p\gamma_l^p}{\gamma_s^p+\gamma_l^p}. \tag{2}$$

The polar and dispersive components of the surface free energy of the test liquids, γ_l^p and γ_l^d, are 50.7 and 22.1 mJ/m^2 for DI water, and 6.7 and 44.1 mJ/m^2 for methylene iodide, respectively. The interfacial free energy, γ_{sl}, was determined based on the equation:

$$\gamma_{sl} = \gamma_s + \gamma_l - \frac{4\gamma_s^d\gamma_l^d}{\gamma_s^d+\gamma_l^d} - \frac{4\gamma_s^p\gamma_l^p}{\gamma_s^p+\gamma_l^p}. \tag{3}$$

The surface roughness was also measured using an optical phase-shifting and white light vertical scanning interferometer (WYKO NT3300).

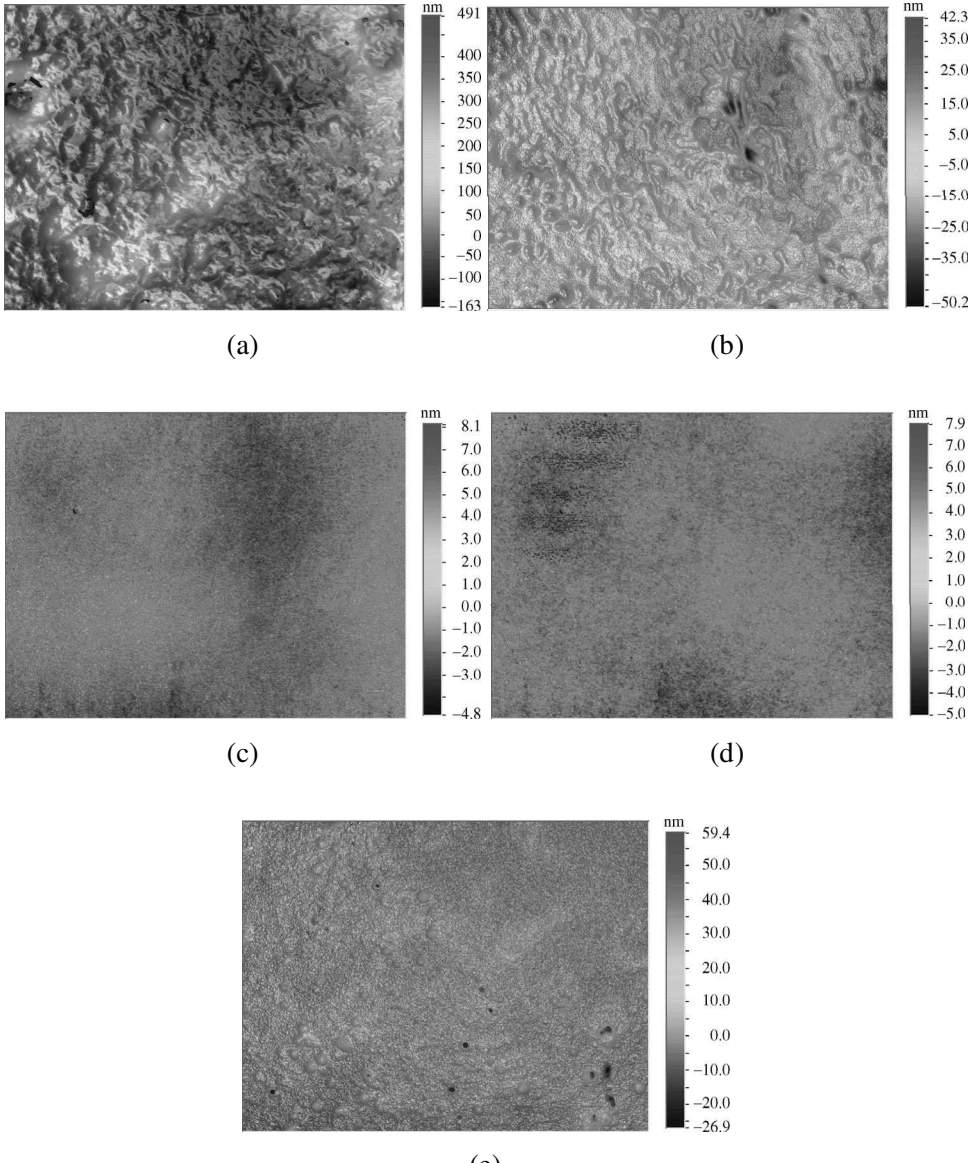

Figure 5. Topographies of the flip-chip component surfaces as determined by a scanning interferometer: (a) polymeric solder mask; (b) eutectic solder; (c) SiO_2 passivation; (d) Si_3N_4 passivation and (e) BCB passivation.

3. INTERFACIAL ADHESION AND FAILURE CHARACTERISTICS OF UNDERFILL WITH PACKAGE COMPONENTS

3.1. Interfacial bond strengths and failure characteristics

The surface topographies of the substrates were examined using a scanning interferometer, as shown in Fig. 5, and Table 3 summarizes the corresponding surface roughness values. It is found that the polymeric solder mask surface was the roughest among all the substrates studied. The roughness of the three different passivation layers was much less than the other substrate surfaces. The roughness of the BCB passivation layer prepared by spin coating was higher than the corresponding roughness of SiO_2 and Si_3N_4 passivation layers prepared by the PECVD technique.

Figure 6 presents the interfacial bond strengths of Underfill A with various package components, along with the corresponding failure modes. The failure mechanisms were studied from the SEM micrographs taken of the fracture surfaces, as shown in Fig. 7, and the typical failure modes derived from the SEM micrographs are schematically illustrated in Fig. 8. The interfacial bond strength between the underfill and solder material was the weakest among the substrates studied, an observation also made by Fan *et al.* [17]. The failure took place predominantly along the underfill-solder interface (Figs 7a and 8a). With such weak interfacial adhesion, the underfill–solder interface is the most likely location where debonding would initiate preferentially during various reliability tests. The bond strength of the underfill–soldermask interface was higher than that of the solder surface, but was generally lower than those for all the three passivation surfaces. The failure occurred by delamination along the solder mask–printed circuit board interface (Figs 7b and 8b). The micrographs in Fig. 7b show a combination of solder mask/PCB debonding and cohesive failure in the solder mask.

Relatively strong interfacial bonds were obtained for all underfill–passivation layers but with different failure behaviors. In particular, the SiO_2 surface imparted the highest interfacial bond strength amongst all the surfaces studied. Delamination occurred between the underfill resin and the SiO_2 or Si_3N_4 passivation surfaces (Fig. 7c), leaving many resin particles onto the substrate fracture surface (Fig. 8c), a typical combination of interfacial and cohesive failures. Strong chemical bonds

Table 3.
Surface roughness of the substrates

Substrate	Average roughness, R_a (nm)
Solder mask	59.99
Eutectic solder	8.79
SiO_2 passivation	0.66
Si_3N_4 passivation	0.64
BCB passivation	2.01

$R_a = \int_0^{l_m} |f(x)|\,dx$; l_m = gauge length; $f(x)$ = surface profile.

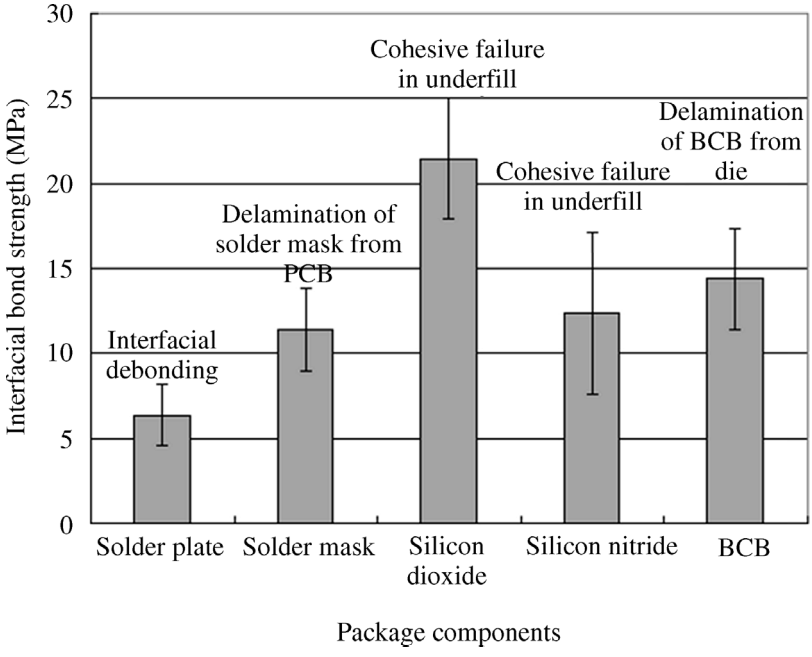

Figure 6. Interfacial bond strengths and loci of failure of underfill A with various package components.

between the organosilane coupling agent added in the epoxy-based underfill and the hydroxyl groups in the passivation layer were mainly responsible for the high underfill-passivation layer interfacial bond strength [7, 18]. In addition, the silanol groups present on SiO_2 or Si_3N_4 passivation layers can form strong covalent bonds with the resin through the formation of Si—O—Si [18], as schematically shown in Fig. 9. The underfill–BCB interface imparted a high interfacial bond strength and the failure occurred mainly along the BCB layer-silicon die interface as seen in Fig. 7e, similar to the schematic failure mode shown in Fig. 8a. The failure surface suggests that the underfill–BCB interface was stronger than the BCB–silicon die interface.

A comparison of the interfacial bond strengths (Fig. 6) with the surface roughness data given in Table 3 suggests that surface roughness was not the predominant factor in determining the interfacial bond strength in the present study. No apparent correlation was established between the interfacial adhesion and the surface roughness data.

3.2. Effect of underfill resin type

Figure 10 presents the results from button shear tests carried out on four different underfill resins. There was no apparent correlation between the interfacial bond strength and failure mode in the button shear test for different resins with respect to different substrate surfaces. However, a general observation is that the conventional

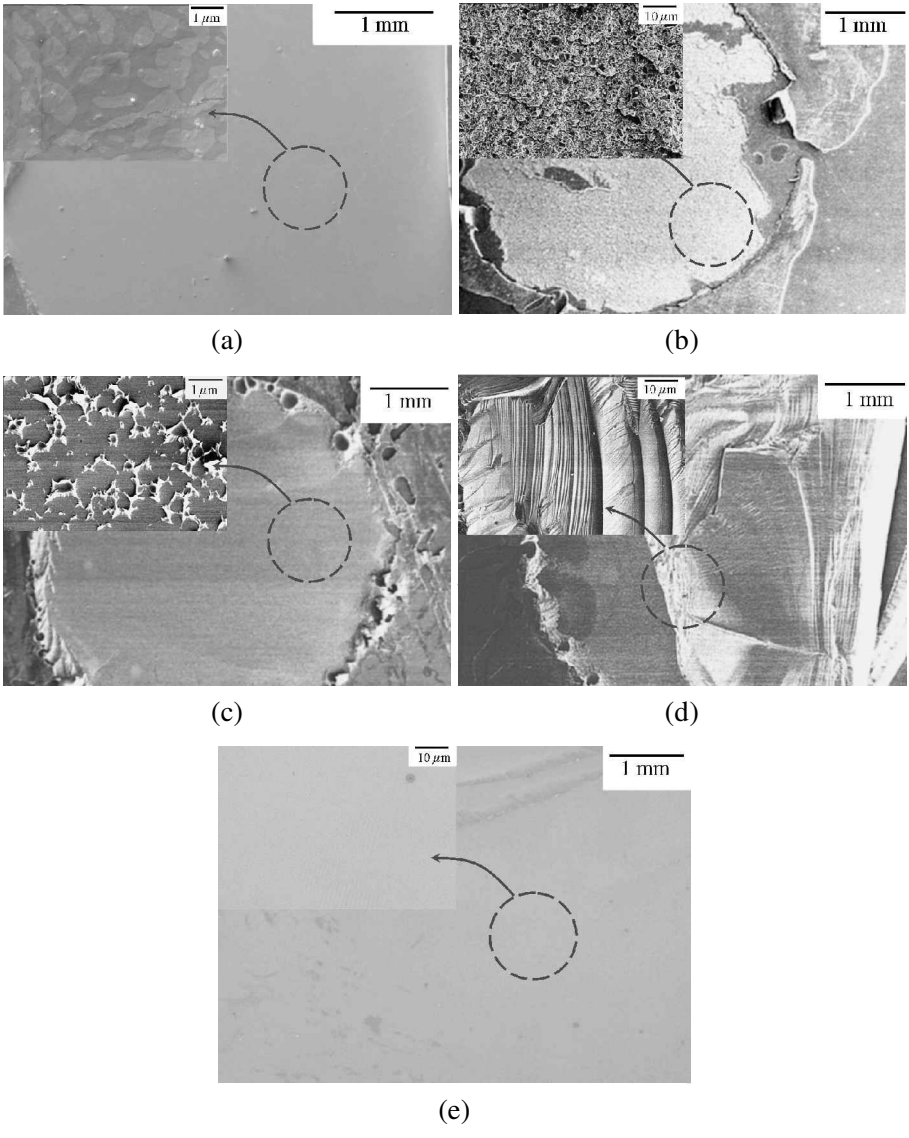

Figure 7. SEM micrographs of fracture surfaces after the button shear test: (a) solder; (b) solder mask; (c) SiO_2 passivation layer with conventional underfill resin (UF A); (d) SiO_2 passivation layer with no-flow underfill resin (UF C) and (e) BCB passivation layer.

underfills (UF A and B) showed stronger adhesion with solder plate and solder mask surfaces than the no-flow underfill resins (UF C and D), while the no-flow underfill resins showed stronger adhesion with the inorganic passivation layer surfaces.

All specimens made from four different resins on the solder plate failed by typical interfacial debonding from the substrate, showing the weakest linkage amongst all surfaces studied. The no-flow underfill resins tended to debond along the interface with solder mask (Fig. 8a), with generally lower interfacial bond strengths than for

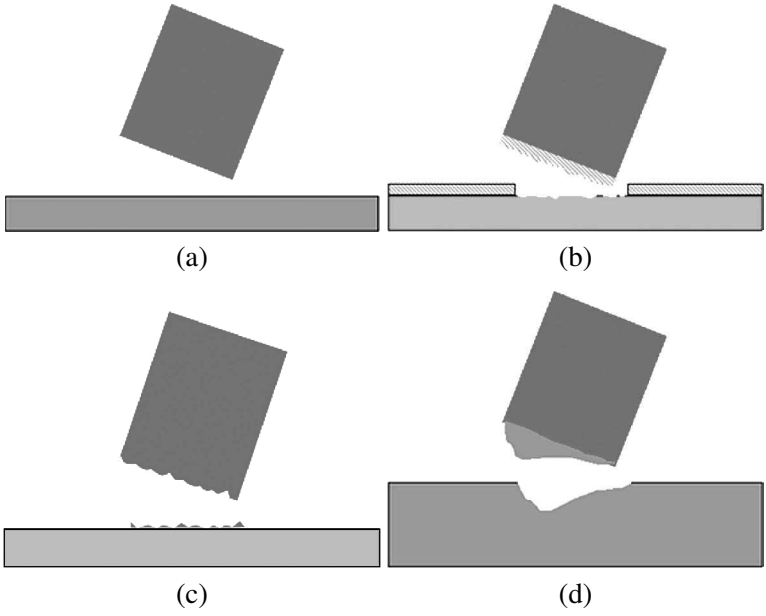

Figure 8. Schematics of different failure modes in the button shear test: (a) interfacial failure; (b) solder mask debonding; (c) combination of interfacial and cohesive failure within underfill and (d) silicon cratering.

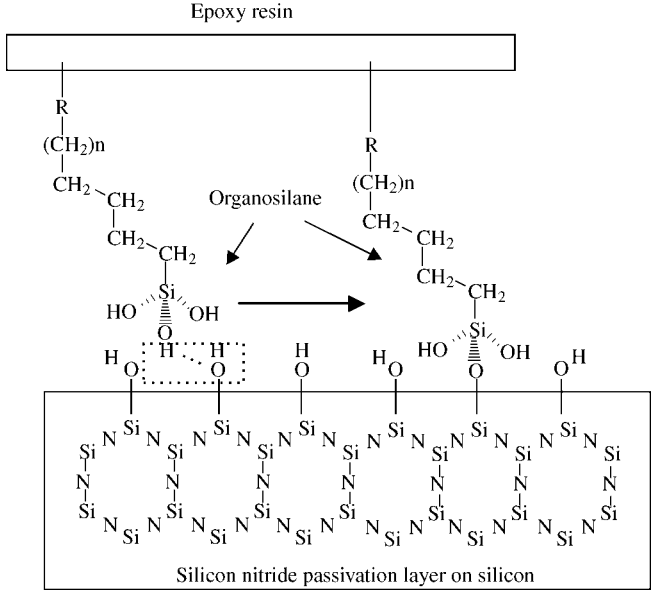

Figure 9. Bonding mechanism of the organosilane in the epoxy resin with silicon nitride passivation layer [18].

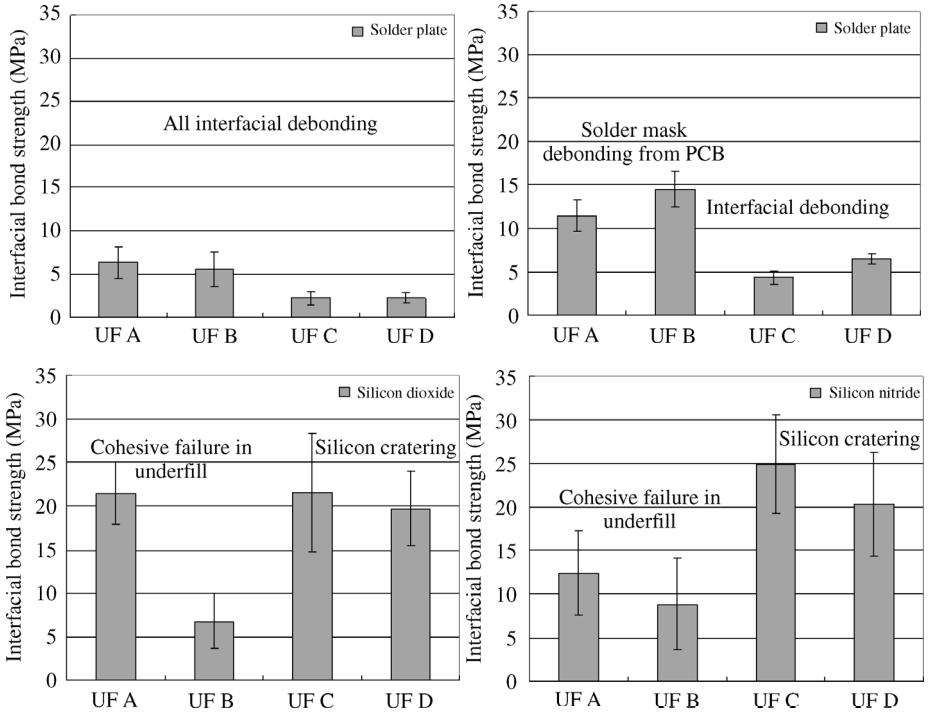

Figure 10. Interfacial bond strength and loci of failure of underfills with various substrates: (a) solder plate; (b) solder mask; (c) SiO_2 passivation and (d) Si_3N_4 passivation.

the conventional underfill resins which showed delamination from the underlying PCB (Fig. 8b). This observation confirmed that the solder mask–PCB interface was more strongly bonded than the underfill resin–solder mask interface. With regard to the specimens bonded to inorganic passivation surfaces, the conventional underfill resin delaminated from the passivation layer leaving many tiny resin particles on the failure surface (see Fig. 7c). The nodular shape of resin particles suggests that significant plastic deformation of the underfill had taken place before delamination. For the no-flow underfill resin specimens, significant cratering fracture was observed in the silicon die (Fig. 7d). It is suspected that large shrinkage introduced in the no-flow underfill resin and the passivation layer was partly responsible for the cratering fracture. The shrinkage stress originates mainly from differential cooling from the curing temperature of the underfill resin and is approximately proportional to the difference in the coefficient of thermal expansion (CTE) between the bonded materials. The CTEs measured in our study based on the thermomechanical analysis (TMA) were 48 ppm/°C and 70/°C, respectively for UF A and UF C. The weight percentage of fused SiO_2 filler in both conventional underfills (UF A and B) was approx. 50%, whereas the no-flow underfills (UF C and UF D) contained a small amount of reactive liquid rubber particles. The absence of rigid particles of very low CTE (typically 0.5 ppm/°C for fused SiO_2)

Table 4.
Polarity of various package component surfaces and cured underfills (in mJ/m^2)

	γ^p	γ^d	γ	Polarity (γ^p/γ)
Solder plate	14.20	29.89	44.09	0.32
As-received solder mask	5.53	30.37	35.90	0.15
SiO_2 passivation	41.66	25.19	66.85	0.62
Si_3N_4 passivation	34.76	26.28	61.04	0.57
Underfill A	11.28	29.74	41.02	0.27
Underfill B	10.24	33.74	43.98	0.23
Underfill C	6.89	40.86	47.75	0.14
Underfill D	14.04	35.27	49.31	0.28

in the no-flow underfill resins was mainly responsible for the high shrinkage in the passivated silicon die and the resulting cratering fracture during the button shear test. The CTE of silicon die is typically 3–5 ppm/°C. UF B exhibited much lower interfacial adhesion with SiO_2 and Si_3N_4 passivation surfaces than the other three resins, although it provided relatively high interfacial bond strengths with solder plate and solder mask surfaces compared to the other resins. It is likely that UF B does not contain a silane coupling agent, which is normally added in the resin for strong chemical interactions with the inorganic die passivation layer.

The surface free energies of the underfill resins and substrates were evaluated from contact angle data. The polar and non-polar (dispersive) components of surface free energies were calculated based on equations (2) and (3), and are summarized in Table 4. The polarity is defined as the ratio of the polar component, γ^p, to the total surface free energy, γ^s, which is associated with the surface wettability in promoting intimate contact between the adhesive and the adherend. The surface polarity was in the order: SiO_2 passivation > Si_3N_4 passivation > solder plate > solder mask. It is expected that an increase in substrate surface polarity gives rise to higher wettability for intimate contact between the substrate and the underfill resin, hence a stronger interfacial bond [13]. This is true for all substrate surfaces, except the organic solder mask surface that showed predominant interfacial failure along the solder mask–PCB interface (Figs 7b and 8b) with higher interfacial bond strength than the underfill–solder interface.

Several thermodynamic parameters have been successfully used to correlate with the practical bond strength (measured adhesion), such as the work of adhesion [19, 20], matching surface free energies [19, 21] and polarities between the adhesive and adherend [16, 19], interfacial tension [16, 19] and spreading coefficient [16, 19], where the spreading coefficient was found to be useful in correlation with the bond strength in the present study as shown below. The spreading coefficient S_{sl} is a measure of the decrease in interfacial free energy per unit area brought about by bringing the two surfaces in contact, and is expressed as:

$$S_{sl} = \gamma_s - \gamma_l - \gamma_{sl}, \tag{4}$$

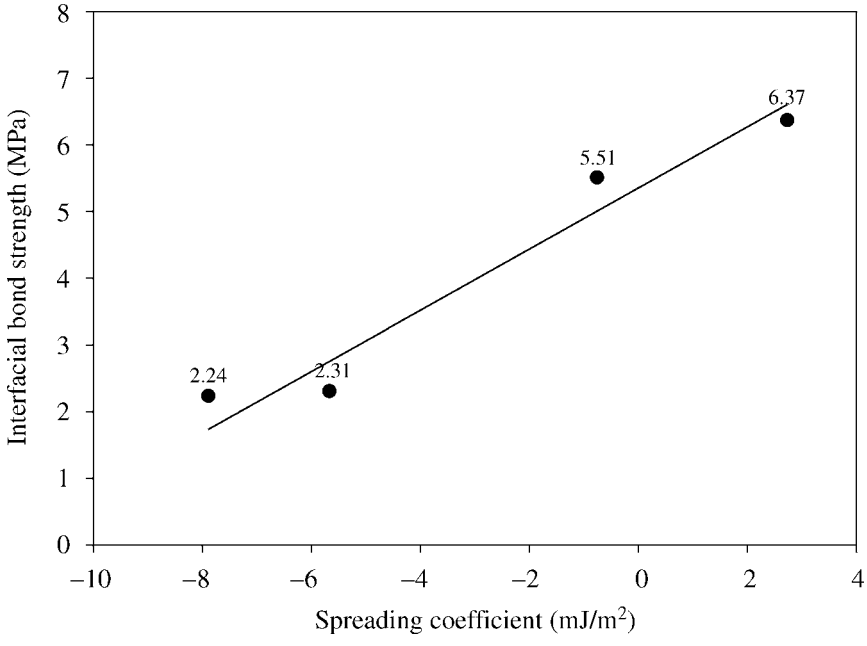

Figure 11. Correlation between interfacial bond strength and spreading coefficient of various underfill resins on solder material.

where the subscripts s and l refer to surface free energies of the solid surface and the liquid, respectively.

A positive spreading coefficient indicates spontaneous spreading of the liquid on the solid surface. Table 5 summarizes the calculated values of these parameters for various combinations of underfill and substrate surfaces. The interfacial bond strengths measured from the button shear tests are also included. Only the underfill–solder plate interface showed interfacial failure in the button shear test (Fig. 8a), which satisfies the requirement for correlating the thermodynamic parameters with the practical bond strength. Therefore, the bond strengths of underfill–solder plate interfaces for four different resins are plotted as a function of the spreading coefficient and an approximately linear correlation was obtained, as shown in Fig. 11. The higher the spreading coefficient, the stronger the interface bond was [16], indicating the importance of spreading coefficient in controlling the adhesion of the underfill–solder plate interface.

4. EFFECTS OF FLUX RESIDUE AND POST-SOLDER REFLOW CLEANING

4.1. Effect of flux residue on adhesion

In this section, the formation of voids and interfacial adhesion with underfill resin both of which are affected by the flux residue on the substrate surface are evaluated. The C-SAM images taken of flip-chip packages with and without post-solder reflow

Table 5.
Thermodynamic adhesion parameters from contact angle analysis

	Underfill A				Underfill B				Underfill C				Underfill D			
	γ_{sl}	W_a	σ	S_{sl}	γ_{sl}	W_a	σ	S_{sl}	γ_{sl}	W_a	σ	S_{sl}	γ_{sl}	W_a	σ	S_{sl}
Solder	0.34	84.77	6.37	2.73	0.87	87.2	5.51	−0.76	4.23	87.61	2.24	−7.89	0.45	92.95	2.31	−5.67
Soldermask	1.97	74.95	8.48	−7.09	1.58	78.3	14.56	−9.66	1.69	81.96	4.33	−13.54	4.06	81.15	6.46	−17.47
SiO_2	17.81	90.06	21.47	8.02	20.26	90.57	6.76	2.61	28.62	85.98	21.60	−9.52	15.38	100.78	19.71	2.16
Si_3N_4	12.19	89.87	12.37	7.83	14.29	90.73	8.87	2.77	21.82	86.97	24.84	−8.53	10.11	100.24	20.38	1.62

γ_{sl} (mJ/m^2) = interfacial free energy, W_a (mJ/m^2) = work of adhesion; σ (MPa) = shear stress (interfacial bond strength); S_{sl} (mJ/m^2) = spreading coefficient.

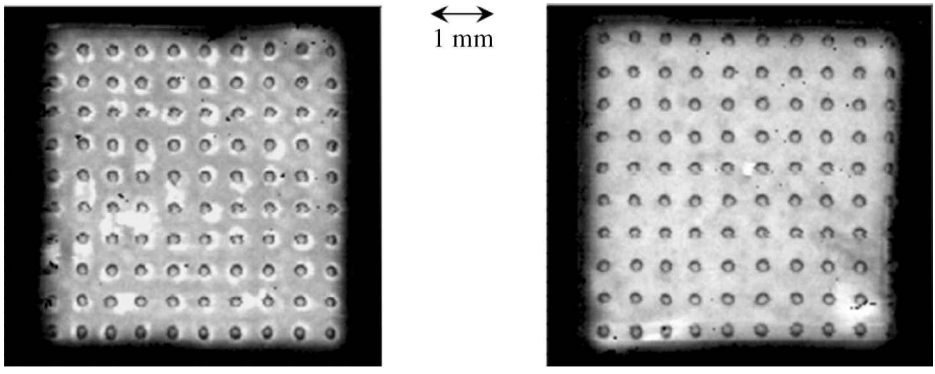

Figure 12. C-SAM images of flip-chip package illustrating the completeness of underfilling by comparing the amounts of voids (in white color) near the solder joints: (a) without post-reflow cleaning and (b) with post-reflow cleaning.

cleaning are compared in Fig. 12. For the flip chip package prepared without cleaning, there were solder balls that were surrounded by areas of white color representing voids (Fig. 12a). It is seen that relatively large amounts of flux residue remained in the package after underfill curing, even though only 20–30 μm thick flux layer was applied on the flip-chip in the present flux dipping method. In fact, similar extents of void occurrence have also been reported in other studies [22, 23], and it appears that the residue with its crystalline and defined structure is not thermally decomposed during the underfill is dispensed and cured [23]. In contrast, such voids were almost absent in the package with post-reflow cleaning, confirming the necessity of post-reflow cleaning to avoid process-induced defects. These voids are known to be detrimental to the reliability and lifetime of FCOB packages [6].

The effects of flux residue and post-reflow cleaning on the interfacial adhesion of the three package surfaces, namely solder, solder mask on PCB and SiO_2 passivation on the die, were then studied. The interfacial bond strengths of these surfaces with underfill resin A for three different surface conditions are compared in Fig. 13. It is obvious that the presence of flux residue on these component surfaces is detrimental to interfacial adhesion with underfill resin. The deterioration of interfacial adhesion was the most severe for the solder (82% reduction), whereas moderate (39% and 52%) reductions were noted for the solder mask and SiO_2 passivation surfaces. Removing the flux from the substrate surfaces with a saponifier followed by DI water rinsing allowed almost full recovery of the original interfacial adhesion. For the solder surface, especially, the interfacial bond strength after cleaning was even higher than that for the as-received condition. This may indicate that the as-received solder had already been contaminated or oxidized upon exposure to the environment. In this regard, routine cleaning is strongly recommended for the solder surface to achieve strong interfacial adhesion before encapsulation with an underfill

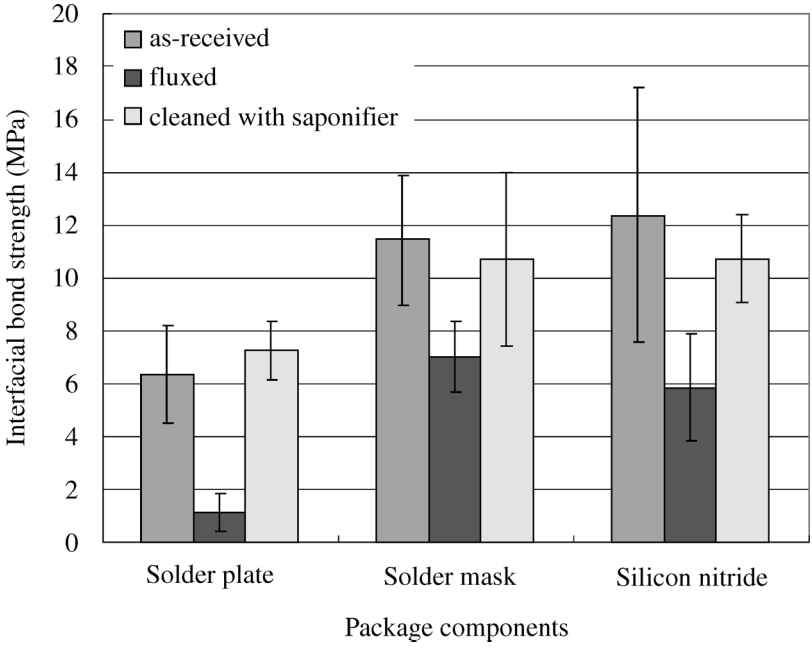

Figure 13. Interfacial bond strength of Underfill A with package components in the presence of flux residue and the effect of cleaning the residue.

resin. Apart from the approach to remove the flux residue for enhancing the underfill adhesion with various package components, the underfill-flux compatibility is also worth studying, as demonstrated by Fan *et al.* [17], in order to eliminate the cleaning process.

4.2. Effect of flux residue on solder failure

Based on the above discussion, the effects of voids in the underfill on the failure mode of FCOB taking place during the reliability test were studied. A comparison of the C-SAM images revealed a few interesting observations. For the package without any post-reflow cleaning before underfilling, voids were accumulated near almost all solder balls and after 1000 cycles the sizes of voids increased significantly, as shown in Fig. 14a. In contrast, for the package with post-reflow cleaning the overall integrity of the underfill adhesion with the package components remained robust and very few additional voids were induced or the void size increased only slightly after thermal cycles as noted in Fig. 14b.

The cross-sectional SEM micrographs shown in Fig. 15 suggested that for the package with voids around the solder due to the lack of post-reflow cleaning, the solder was severely deformed after cyclic loading. The irregular, inelastic deformation of solder even led to the formation of many voids within the solder ball, caused by the lack of mechanical coupling between the silicon die and substrate from the surrounding underfill resin. In contrast, for the package with post-reflow

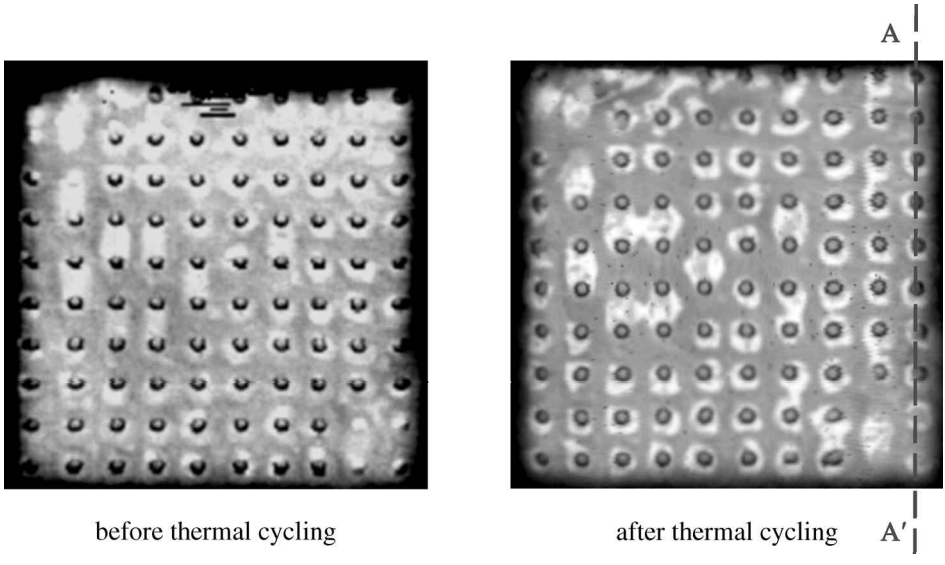

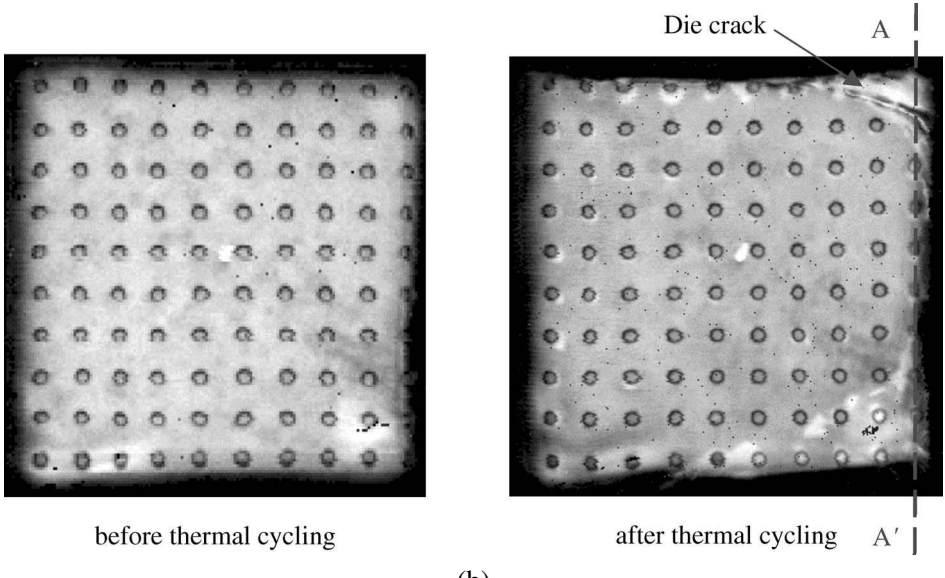

Figure 14. Comparisons of the delamination patterns in FCOB packages after thermal cycling test by C-SAM microscopy: (a) without post-reflow cleaning and (b) with post-reflow cleaning (A–A′: cross section).

cleaning and complete underfilling with only a few voids, the solder joints were undeformed after thermal cycling due to the reinforcing nature of the encapsulant. The solder joints remained intact, in spite of the development of microcracks which developed along the solder–under bump metallization (UBM) interface. This

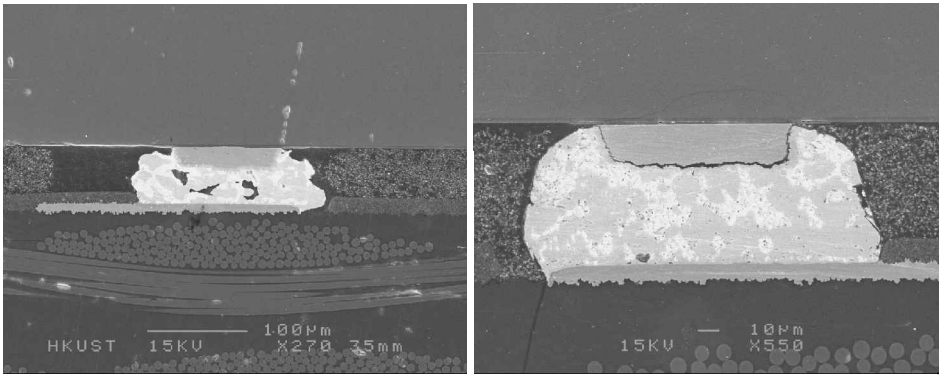

(a) (b)

Figure 15. Cross-sectional SEM micrographs of FCOB package after 1000 cycles showing the differences in failure modes of the solder joints: (a) without post-reflow cleaning; (b) with post-reflow cleaning.

failure mode arises from creep fatigue at high temperatures encountered during thermal cycling. This observation has been attributed to the hydrostatic stresses in the solder generated during the underfill resin curing. The cracks in the solder joints then propagate in a slow and stable manner with an extended life [23]. Cracking in the PCB was also noticed in the micrograph, which arose from the extensive stress concentration at the solder joint corner. However, even with the poor interfacial adhesion with the underfill resin and many voids surrounding the solder joints as demonstrated in the two micrographs, the packages are expected to still function well without showing any failure under mild operating conditions like the working conditions in domestic appliances.

5. CONCLUSIONS

The interfacial adhesion characteristics between the underfill and the flip chip package components, i.e. silicon die passivation layer, epoxy-based solder mask and eutectic solder, were evaluated. The importance of cleaning the fluxed surface after solder reflow has been shown. The following conclusions are drawn from the present study:

(1) All underfill resins exhibited the weakest interfacial bond strength with solder, showing preferential delamination along the underfill/solder interface when the package was subjected to cyclic loading.

(2) Most of the underfill resins showed better interfacial bond strengths with passivation layers than with solder mask.

(3) The presence of flux residue deteriorated significantly the underfill adhesion performance with all package components studied. Cleaning the surface using a saponifier was efficient in restoring the original interfacial bond strength.

(4) The failure mechanisms of solder joints in FCOB packages were found to be strongly dependent on the presence of voids, which, in turn, was determined by whether the fluxed surface was cleaned or not.

Acknowledgements

The work described in this paper was partially supported by grants from the Research Grants Council of the Hong Kong Special Administrative Region, China. Thanks are due to Daeduck Electronics Co., South Korea (Mr. J. H. Lee) for the supply of solder masked printed circuit boards used in this study. Technical supports from the Materials Characterization and Preparation Facilities (MCPF), Advanced Engineering Materials Facilities (AEMF) and EPack Laboratory of HKUST are appreciated.

REFERENCES

1. J. B. Nysaether, P. Lundstrom and J. Liu, *IEEE. Trans. Comp. Packag. Manufact. Technol. Part A* **21**, 281–287 (1998).
2. J. Lu, A. Trigg, J. Wu and T. Chai, *Int. J. Microcircuits Electron. Packag.* **21** (3), 231–235 (1998).
3. L. Fan, K. S. Moon and C. P. Wong, *J. Adhesion Sci. Technol.* **16**, 213–223 (2002).
4. D. R. Gamota and C. M. Melton, *Circuit World* **24** (1), 7–12 (1997).
5. C. E. Park, B. J. Han, H. E. Bair and V. Reddy Raju, *J. Mater. Sci. Lett.* **16**, 1027–1029 (1997).
6. R. Tummala (Ed.), *Fundamentals of Microsystems Packaging.* McGraw-Hill, New York, NY (2001).
7. Q. Yao, J. Qu, J. Wu and C. P. Wong, *IEEE Trans. Electron. Packag. Manufact.* **22** (4), 264–267 (1999).
8. S. Y. Y. Leung, S. Luo, D. C. C. Lam and C. P. Wong, in: *Proc. IEEE 50th Electronic Component and Technology Conference*, pp. 581–585 (2000).
9. S. Luo and C. P. Wong, in: *Proc. IEEE 50th Electronic Component and Technology Conference*, pp. 311–317 (2000).
10. C. Lee, R. Gopalakrishnan, K. Nyunt, A. Wong, R. C. E. Tan and J. W. Ong, *Microelectron. Reliab.* **39**, 97–105 (1999).
11. S. Yi, L. Shen, J. K. Kim and C. Y. Yue, *J. Adhesion Sci. Technol.* **14**, 93–105 (2000).
12. S. Yi, J. K. Kim, C. Y. Yue and J. H. Hsieh, *J. Adhesion* **73**, 1–17 (2000).
13. S. Luo and C. P. Wong, *IEEE Trans. Comp. Packag. Technol.* **24**, 43–49 (2001).
14. M. Lebbai, J. K. Kim, W. K. Szeto, M. M. F. Yuen and P. Tong, *J. Electron. Mater.* **32**, 558–563 (2003).
15. J. S. Hwang, *Modern Solder Technology for Competitive Electronics Manufacturing*, Chapter 8. McGraw Hill, New York, NY (1996).
16. S. Wu, *J. Adhesion* **5**, 39–55 (1973).
17. L. Fan, C. K. Tison and C. P. Wong, *IEEE Trans. Adv. Packag.* **25**, 473–480 (2002).
18. X. Dai, M. V. Brillhart, M. Roesch and P. S. Ho, *IEEE Trans. Comp. Packag. Technol.* **23**, 117–127 (2000).
19. K. L. Mittal, in: *Adhesion Science and Technology*, L.-H. Lee (Ed.), Part A, pp. 129–168. Plenum Press, New York, NY (1975).
20. G. S. Ganesan, G. L. Lewis and H. M. Berg, *Proc. Adv. Elect. Packag. ASME* **EEP-Vol. 10-2**, 717–722 (1995).

21. W. Gutowski, in: *Controlled Interphases in Composite Materials*, H. Ishida (Ed.), pp. 505–520. Elsevier, Amsterdam (1990).
22. C. Beddingfield and L. M. Higgins, III, *IEEE. Trans. Comp. Packag. Manufact. Technol. Part C* **21**, 189–195 (1998).
23. F. Zhang, M. Li, W. T. Chen and K. S. Chian, *IEEE Trans. Comp. Packag. Manufact. Technol.* **26**, 233–238 (2003).